Organic LETTERS

Letter

pubs.acs.org/OrgLett

4,9-Dihydro-4,4,9,9-tetrahexyl-*s*-indaceno[1,2-*b*:5,6-*b*′]dithiophene as a π-Spacer of Donor−π−Acceptor Dye and Its Photovoltaic Performance with Liquid and Solid-State Dye-Sensitized Solar Cells

Liping Cai,[†] Thomas Moehl,[‡] Soo-Jin Moon,[‡] Jean-David Decoppet,[‡] Robin Humphry-Baker,[‡] Zhaosheng Xue,[†] Liu Bin,[†,*] Shaik M Zakeeruddin,*[,‡] and Michael Grätzel*[,‡]

[†]Department of Chemical and Biomolecular Engineering, National University of Singapore, Singapore 117576, Singapore

[‡]Laboratory for Photonics and Interfaces, Institute of Chemical Sciences and Engineering, Swiss Federal Institute of Technology, CH-1015 Lausanne, Switzerland

Supporting Information

ABSTRACT: A new D−π-A organic dye, LC-5, containing 4,9-dihydro-4,4,9,9-tetrahexyl-*s*-indaceno[1,2-*b*:5,6-*b*′]-dithiophene as a novel π-conjugated spacer has been synthesized and tested as a sensitizer in dye-sensitized solar cells (DSC). Volatile and ionic liquid electrolytes have been used in conjunction with the synthesized dye, and the electrolyte influence on the photovoltaic performance of DSCs was investigated. A detailed investigation, including transient photocurrent/photovoltage decay measurements and electrochemical impedance spectroscopy data, provide important conclusions about the influence of electrolytes on the photovoltaic parameters.

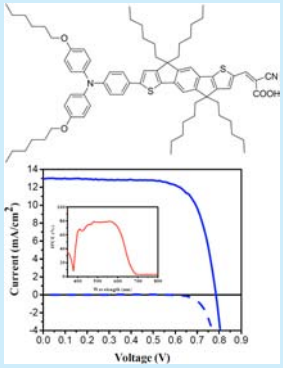

Dye-sensitized solar cells (DSCs) have been investigated extensively as potential candidates for renewable-energy systems due to high efficiency and low cost.[1] Ruthenium complexes developed as sensitizers for DSCs have reached solar to electrical power conversion efficiencies (PCE) over 11%.[2] Organic dyes have attracted attention because of the flexibility in design and synthesis. Of particular interest are sensitizers employing indoline,[3] squarylium,[4] porphyrin chromophores,[5] and the wide family of π-bridged donor−acceptor (D−π-A) dyes[6] which have attained PCEs of around 10%.[7] A record power conversion efficiency of 12.3% was reached using a push−pull zinc porphyrin with an organic cosensitizer and cobalt redox electrolyte.[5b]

Many DSC organic sensitizers feature three typical parts, i.e., a donor, π-conjugated spacer and an acceptor/anchoring group. A strong electronic coupling across the bridge is essential for light-induced charge separation and vectorial electron transfer. To safeguard high electron-transfer rates within the molecule the π-conjugated spacer plays a critical role. Several synthetic strategies for the development of donors and π-conjugated spacers of D−π−A dyes have been explored to extend their absorption spectra to longer wavelengths and/or to increase their molar absorption cross-section.[8] In this study, we are introducing 4,9-dihydro-4,4,9,9-tetrahexyl-*s*-indaceno[1,2-*b*:5,6-*b*′]-dithiophene as a novel π-conjugated spacer of a D−π−A dye.

The synthetic route to LC-5 is shown in Scheme 1. 4, 9-Dihydro-*s*-indaceno[1,2-*b*:5,6-*b*′]dithiophene (**1**) was prepared according to previous reports.[9] Four alkyl chains were introduced into compound **1** under base conditions to obtain 4,9-dihydro-4,4,9,9-tetrahexyl-s-indaceno[1,2-b:5,6-b′]-dithiophene (**2**) in 70% yield. 4, 9-Dihydro-4,4,9,9-tetrahexyl-s-indaceno[1,2-*b*:5,6-*b*′]-dithiophene-2-carbaldehyde (**3**) was obtained in 55% yield by the reaction of compound **2** with $POCl_3$ and DMF in 1,2-dichloroethane solution. The amount and the speed of dropping $POCl_3$ should be controlled to decrease the yield of dithiophene dialdehyde byproduct. By treatment of compound **3** with *N*-bromosuccinimide (NBS) in

Scheme 1. Synthetic Route to LC-5 Dye and Chemical Structure of C218

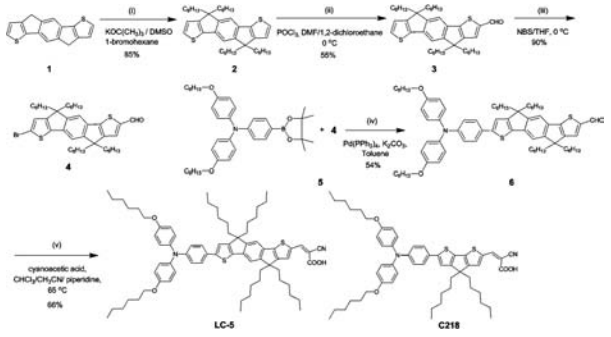

Received: October 28, 2013
Published: December 11, 2013

   dx.doi.org/10.1021/ol402749s | *Org. Lett.* 2014, 16, 106−109

THF solution, 7-bromo-4,9-dihydro-4,4,9,9-tetrahexyl-*s*-indaceno[1,2-*b*:5,6-*b*′]-dithiophene-2-carbaldehyde (**4**) was obtained in 90% yield. The synthetic procedure for 4,4,5,5-tetramethyl-2-[4-[*N*,*N*-bis(4-hexyloxyphenyl)amino]phenyl]-1,3,2-dioxaborolane (**5**) is adapted from a previous publication.[7b] Suzuki coupling was chosen to connect the donor unit **5** and the spacer unit **4** together, which yielded the dye precursor 6-[4-[*N*,*N*-bis(4-hexyloxyphenyl)amino]phenyl]-4,9-dihydro-4,4,9,9-tetrahexyl-*s*-indaceno [1,2-*b*:5,6-*b*′]dithiophene-2-carbaldehyde (**6**) in 55% yield. Knoevenagel condensation between **6** and cyanoacetic acid led to the target dye molecule of 2-cyano-3-[6-[4-[*N*,*N*-bis(4-hexyloxyphenyl)amino]phenyl]-4,9-dihydro-4,4,9,9-tetrahexyl-*s*-indaceno[1,2-*b*:5,6-*b*′]-dithiophene-2-yl]acrylic acid (**LC-5**) in 66% yield. NMR and mass spectra have verified the correct chemical structures of the precursors and the final sensitizer. The molecular structure of **LC-5** and C218 dyes are shown in Scheme 1(enlarged Scheme 1 is shown as Scheme S1 in the Supporting Information). The absorption and emission spectrum of **LC-5** adsorbed on the surface of thin TiO_2 film are shown in Figure S1 (Supporting Information). UV−vis absorption spectra of the **LC-5** dye in CH_2Cl_2 solution in the protonated and deprotonated form are depicted in Figure S2 (Supporting Information). The absorption peak maxima and as well as the molar absorption coefficients are summarized in Table S1 (Supporting Information). In general, D−π−A dyes in solution show peaks in the visible and UV region corresponding to intramolecular charge transfer and $\pi-\pi^*$ transitions, respectively. For **LC-5** which features 4,9-dihydro-4,4,9,9-tetrahexyl-*s*-indaceno[1,2-*b*:5,6-*b*′]dithiophene as a spacer the molar absorption coefficient is 75800 cm^{-1} at 520 nm. The deprotonated dye has a molar absorption coefficient of 98000 cm^{-1} at 481 nm. The molar absorption coefficient of C218 dye is 62700 at 555 nm, which has 4,4-dihexyl-4*H*-cyclopenta[2,1-*b*:3,4-*b*]dithiophene as a π-spacer.[7b] The 30 nm blue shift of **LC-5**'s absorption maxmium compared to C218, despite more extended conjugation, can be explained by the energetically demanding uplifting of the resonance energy of the benzene ring in **LC-5**. Conversely, the extension of π-spacer conjugation does increase the molar absorption coefficient for the low energy intramolecular charge transfer transition of **LC-5**. When **LC-5** is adsorbed on TiO_2, the maximun absorption peak is blue-shifted by around 40 nm compared to that in solution. A similar trend was also observed with C218 dye in the adsorbed state,[7b] and can be explained by the deprotonation of −COOH group on the surface of the TiO_2 film. This is supported by the observation that the spectrum of the adsorbed sensitizer perfectly matches that of the deprotonated dye in solution (Figure S1, Supporting Information).[7a]

Cyclic voltammetry was employed to elucidate the redox behavior of **LC-5.** The results are found in Table S1 (Supporting Information). A reversible couple at 0.87 V vs NHE indicates that there is enough driving force for the dye regeneration with an iodide/triiodide redox electrolyte (redox potential of ∼0.4 V vs NHE). The excited state reduction potential of **LC-5** dye was obtained by combining the oxidation potential with the energy of the transition upon light absorption. The excited state potential is sufficiently above the TiO_2 conduction band edge (−0.5 V vs NHE). This ensures efficient electron injection.

To obtain more insight into the molecular structure and electron distribution within the molecule, DFT calculations were performed. The molecules were simplified by replacing alkyl chains with methyl groups to reduce the number of basis functions. Initial optimization of the geometry of the molecules reveals that the triphenylamine donor is slightly distorted from planarity with the π-spacer. As shown in Figure S3 (Supporting Information), the HOMO orbitals are mainly located at the donor end of the molecule. There is some extension of the HOMO onto the π-conjugated building block. Nevertheless, the LUMO is confined to the π-bridge and acceptor, favoring light induced charge separation and subsequent electron injection into the titania conduction band.

The photovoltaic performance of LC-5 dye was evaluated in DSCs by utilizing two types of electrolytes. Device A employs a volatile solvent (Z960) while B is based on an ionic liquid electrolyte (Z952). The photocurrent−voltage (J-V) curve of device A is shown in Figure 1 and the PV parameters i.e. the

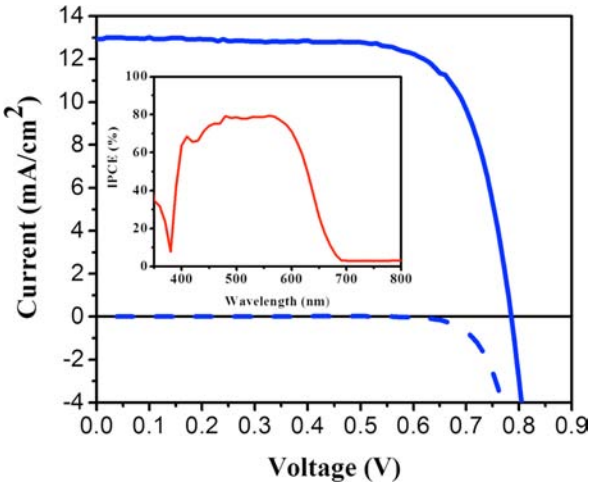

Figure 1. Photocurrent density−voltage characteristics of device A under AM 1.5G illumination (100 mW cm^{-2}). The inset shows the IPCE of device A. Cells were tested using a mask with an aperture area of 0.187 cm^2.

open-circuit photovoltage (Voc), short-circuit photocurrent density (Jsc), fill factor (FF) and solar-to-electrical power conversion efficiency (PCE) are tabulated in Table S2 (Supporting Information). A PCE of 7.5% was obtained with device A. Whereas for B, a 6.9% PCE was obtained under AM 1.5G sunlight (100 mW/cm^2). The inferior PCE of device B compared to A results from lower Jsc and Voc values. The incident monochromatic photon-to-electric-current conversion efficiency (IPCE) spectrum for device A is shown as an inset in Figure 1. The IPCE spectrum shows a broad response in the range of 450 to 600 nm and a maximum value of 80% was reached at 500 nm. The Jsc values obtained from calculating the integral overlap of the IPCE spectrum with the standard AM 1.5G solar spectral solar photo flux are close to the measured Jsc values showing that any spectral mismatch between the simulated and true AM 1.5 solar emission is negligibly small. When a transparent TiO_2 film (2.9 μm) was applied in combination with LC-5 and Z960, an impressive 5.8% PCE was obtained.

To understand the variations in the photovoltaic parameters of devices A and B, we employed electrochemical impedance spectroscopy (EIS) measurements in the dark. In addition, transient photocurrent and photovoltage decay measurements were utilized to compare the rates of interfacial recombination of electrons from the TiO_2 conduction band to the oxidized

dx.doi.org/10.1021/ol402749s | *Org. Lett.* 2014, 16, 106−109

form of the redox couple (triiodide) present in the electrolytes. It is known that the electrolyte composition has significant influence on the photovoltaic performance of DSC devices due to ionic concentration (and its corresponding redox potential), diffusion rate, interface formation and cationic screening effects.

The dark current of the devices plotted against applied potential is shown in Figure S4 (Supporting Information). The difference in the dark currents of the devices A and B at lower forward bias is mainly related to the difference in interface formation (FTO/electrolyte) at the photoanode. In the case of device A, the exchange current density is higher, which leads to a lower charge transfer resistance at the interface when compared to device B. The dark current behavior changes as soon as the TiO_2 becomes more conductive and dominates the current voltage response. The origin for the different behavior of these types of devices at higher forward bias might be originating from the differences in the recombination rates and/or a shift in the conduction band edge (E_{CB}) of the TiO_2 films. Another feature of the dark current of the device B is the limiting of the current at higher forward bias (i.e., deviation from exponential behavior at higher potentials) due to the lower diffusion coefficient of the triiodide in the viscous ionic liquid electrolyte causing a higher IR drop. To further evaluate this observation, EIS measurements were performed and analyzed according to the transmission line model.[10]

In the EIS analysis of the DSC devices several features can be observed in Figure S5 (Supporting Information). The charge transfer resistance at the Pt/electrolyte interface is slightly lower for device A compared to device B. The Warburg diffusion resistance for device B is about 8 to 9 times higher at higher current densities, which causes the dark current to saturate at higher forward biases.

Figure 2 presents the transport and the recombination resistance as well as the chemical capacitance of the TiO_2 for

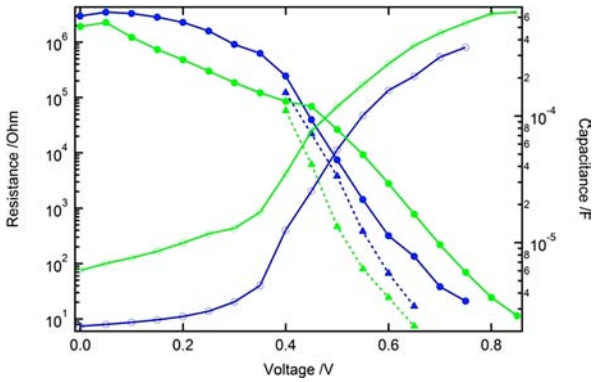

Figure 2. Charge-transfer resistance at the dye-sensitized TiO_2/electrolyte interface (filled circles), the transport resistance for the electrons inside the TiO_2 (filled triangles), and the chemical capacitance of the TiO_2 (open circles) determined by EIS for device A (green) and device B (blue).

devices A and B determined by EIS. At low forward potential, the recombination resistance represents the charge transfer resistance at the FTO/electrolyte interface of the photoanode. As expected by the trend of the dark currents, at low forward bias, the lower initial value and the faster decrease of the charge transfer resistance at the TiO_2/electrolyte interface for device A accounts for the higher dark current observed (Figure S4 (Supporting Information) and Figure 2). At higher forward potentials the situation is reversed and the charge transfer resistance of device B diminishes quickly as the TiO_2 becomes electronically more conductive. The slope of the R_{ct} at higher forward bias is dominated by recombination kinetics of the electrons from the mesoporous TiO_2 film with the triiodide ion presented in the electrolyte. R_{ct} is defined by $R_{ct} = R_{0,ct} \exp(-qV/K_BT)$, where β is the transfer coefficient describing the reaction order of the recombination process (q, elementary charge; k_B, Boltzmann constant; T, temperature; V, voltage). The β values attributed for devices B and A are 0.75 and 0.60, respectively. β is directly related to the diode ideality factor ($m = 1/\beta$), yielding 1.33 and 1.66 for device B and device A, respectively. Such a variation in the recombination behavior of two DSC devices is not surprising, since the conduction band is influenced by the interface formation at the TiO_2/ electrolyte contact as well as by the interaction of surface states with the triiodide ions. Therefore, the balance between the recombination through conduction band electrons and the recombination coming from surface states leads to the different β values and diode ideality factors.[11]

For device A, the chemical capacitance indicates a lower lying conduction band edge of the TiO_2 (~60 mV lower when compared to device B) even though the dark current at higher forward bias is lower than that of the device B. This finding implies a much longer electron lifetime and higher charge collection efficiency in device A. The shift of the TiO_2 conduction band edge stems from the presence of Li^+ ions in the electrolyte Z960 (device A). A similar effect is also observed following transient measurements, but to a lesser extent (38 mV, Figure S6, Supporting Information).

To compare the electron lifetime, the chemical capacitance was chosen as the reference base for the fermi energy (E_f), since the change in trap distribution is relatively small as visible by the shape of the density of states (DOS) in Figure S6 (Supporting Information). This is superior to plotting against the applied potential or against the conductivity of the TiO_2 as shifts in TiO_2 conduction band, different redox potential of the electrolytes and changes in electron diffusion coefficient inside of the TiO_2 film[12] render these methods less accurate.

In Figures S7 and S8 (Supporting Information), the electron lifetime (and the transport time in case of the EIS measurements) is plotted versus the chemical capacitance. Both EIS and transient photovoltage and photocurrent decay measurements show a longer electron lifetime for device A compared to device B. This explains the observed ~80 mV higher values of Voc for device A in comparison to device B, despite the fact that the conduction band of the TiO_2 is slightly lower in device A.

LC-5 dye was also employed as a sensitizer in a solid-state dye sensitized solar cell (ssDSC) using Spiro-MeOTAD as a hole transport material (labeled as device C). The IPCE of the ssDSC exceeds 65% from 440 to 570 nm, reaching a maximum of 72% at 450 nm as shown in Figure S9 (Supporting Information). The photovoltaic parameters of this ssDSC are tabulated in Table S1 (Supporting Information). The PCE of device C reached 6.1% under an illumination of the AM 1.5G full sunlight (100 mW/cm^2), and at a lower sunlight intensity (10 mW/cm^2) it reached as high as 6.4%.

■ ASSOCIATED CONTENT

Supporting Information

Experimental procedures. This material is available free of charge via the Internet at http://pubs.acs.org.

dx.doi.org/10.1021/ol402749s | Org. Lett. 2014, 16, 106–109

AUTHOR INFORMATION

Corresponding Authors

*E-mail: cheliub@nus.edu.sg.
*E-mail: shaik.zakeer@epfl.ch.
*E-mail: michael.graetzel@epfl.ch.

Notes

The authors declare no competing financial interest.

ACKNOWLEDGMENTS

We thank Dr. Carole Grätzel (Laboratory for Photonics and Interfaces, Swiss Federal Institute of Technology, Lausanne) for fruitful discussions. We thank the Singapore−Berkeley Research Institute for Sustainable Energy (R-279-000-393-592) and the Swiss National Science Foundation for financial support. This work was also supported by the European Research Council (ECR) advanced grant agreement (no. 247404) funded under the "MESOLIGHT" project.

REFERENCES

(1) (a) O'Regan, B.; Grätzel, M. *Nature* **1991**, *353*, 24. (b) Grätzel, M. *Acc. Chem. Res.* **2009**, *42*, 1788−1798.

(2) (a) Chen, C.-Y.; Wang, M.; Li, J.-Y.; Pootrakulchote, N.; Alibabaei, L.; Ngoc-le, C.-h.; Decoppet, J.-D.; Tsai, J.-H.; Grätzel, C.; Wu, C.-G.; Zakeeruddin, S. M.; Grätzel, M. *ACS Nano* **2009**, *3*, 3103. (b) Yu, Q.; Wang, Y.; Yi, Z.; Zu, N.; Zhang, J.; Zhang, M.; Wang, P. *ACS Nano* **2010**, *4*, 6032.

(3) (a) Horiuchi, T.; Miura, H.; Sumioka, K.; Uchida, S. *J. Am. Chem. Soc.* **2004**, *126*, 12218. (b) Akhtaruzzaman, M.; Islam, A.; Yang, F.; Asao, N.; Kwon, E.; Singh, S. P.; Han, L.; Yamamoto, Y. *Chem. Commun.* **2011**, *47*, 12400. (c) Zhu, W.; Wu, Y.; Wang, S.; Li, W.; Li, X.; Chen, J.; Wang, Z.-S.; Tian, H. *Adv. Funct. Mater.* **2011**, *21*, 756.

(4) (a) Yum, J.-H.; Walter, P.; Huber, S.; Rentsch, D.; Geiger, T.; Nüesch, F.; De Angelis, F.; Grätzel, M.; Nazeeruddin, M. K. *J. Am. Chem. Soc.* **2007**, *129*, 10320. (b) Maeda, T.; Hamamura, Y.; Miyanaga, K.; Shima, N.; Yagi, S.; Nakazumi, H. *Org. Lett.* **2011**, *13*, 5994. (c) Yan, Z.; Xu, H.; Guang, S.; Zhao, X.; Fan, W.; Liu, X. Y. *Adv. Funct. Mater.* **2012**, *22*, 345. (d) Li, J.-Y.; Chen, C.-Y.; Ho, W.-C.; Chen, S.-H.; Wu, C.-G. *Org. Lett.* **2012**, *14*, 5420. (f) Shi, Y.; Hill, R. B. M.; Yum, J.-H.; Dualeh, A.; Barlow, S.; Grätzel, M.; Marder, S. R.; Nazeeruddin, M. K. *Angew. Chem.* **2011**, *123*, 6749.

(5) (a) Bessho, T.; Zakeeruddin, S. M.; Yeh, C.-Y.; Diau, E. W.-G.; Grätzel, M. *Angew. Chem., Int. Ed.* **2010**, *49*, 6646. (b) Yella, A.; Lee, H.-W.; Tsao, H. N.; Yi, C.; Chandiran, A. K.; Nazeeruddin, M. K.; Diau, E. W.-G.; Yeh, C.-Y.; Zakeeruddin, S. M.; Grätzel, M. *Science* **2011**, *334*, 629. (c) Chang, Y.-C.; Wang, C.-L.; Pan, T.-Y.; Hong, S.-H.; Lan, C.-M.; Kuo, H.-H.; Lo, C.-F.; Hsu, H.-Y.; Lin, C.-Y.; Diau, E. W.-G. *Chem. Commun.* **2011**, *47*, 8910.

(6) Marszalek, M.; Nagane, S.; Ichake, A.; Humphry-Baker, R.; Paul, V.; Zakeeruddin, S. M.; Gratzel, M. *J. Mater. Chem.* **2012**, *22*, 889.

(7) (a) Zeng, W.; Cao, Y.; Bai, Y.; Wang, Y.; Shi, Y.; Zhang, M.; Wang, F.; Pan, C.; Wang, P. *Chem. Mater.* **2010**, *22*, 1915. (b) Li, R.; Liu, J.; Cai, N.; Zhang, M.; Wang, P. J. *Phys. Chem. B* **2010**, *114*, 4461.

(8) (a) Mishra, A.; Fischer, M. K. R.; Bäuerle, P. *Angew. Chem., Int. Ed.* **2009**, *48*, 2474. (b) Hagfeldt, A.; Boschloo, G.; Sun, L.; Kloo, L.; Pettersson, H. *Chem. Rev.* **2010**, *110*, 6595. (c) José, M. S.; Emilio, A.; Julian, D. G.; Alberto, G.; Javier, J.; Pablo, O.; Daniel, S.-P. *J. Phys.: Condens. Matter* **2002**, *14*, 2745.

(9) Zhang, W.; Smith, J.; Watkins, S. E.; Gysel, R.; McGehee, M.; Salleo, A.; Kirkpatrick, J.; Ashraf, S.; Anthopoulos, T.; Heeney, M.; McCulloch, I. *J. Am. Chem. Soc.* **2010**, *132*, 11437.

(10) (a) Fabregat-Santiago, F.; Bisquert, J.; Garcia-Belmonte, G.; Boschloo, G.; Hagfeldt, A. *Sol. Energy Mater. Sol. Cells* **2005**, *87*, 117. (b) Fabregat-Santiago, F.; Garcia-Belmonte, G.; Mora-Sero, I.; Bisquert, J. *Phys. Chem. Chem. Phys.* **2011**, *13*, 9083.

(11) (a) Xu, X.; Cao, K.; Huang, D.; Shen, Y.; Wang, M. *J. Phys. Chem. C* **2012**, *116*, 25233. (b) Wang, H.; Peter, L. M. *J. Phys. Chem. C* **2012**, *116*, 10468.

(12) Nakade, S.; Kambe, S.; Kitamura, T.; Wada, Y.; Yanagida, S. *J. Phys. Chem. B* **2001**, *105*, 9150.